

Phonon spectral function of the one-dimensional Holstein-Hubbard model

Manuel Weber, Fakher F. Assaad, and Martin Hohenadler

Institut für Theoretische Physik und Astrophysik, Universität Würzburg, 97074 Würzburg, Germany

(Dated: March 2, 2024)

We use the continuous-time interaction expansion (CT-INT) quantum Monte Carlo method to calculate the phonon spectral function of the one-dimensional Holstein-Hubbard model at half-filling. Our results are consistent with a soft-mode Peierls transition in the adiabatic regime, and the existence of a central peak related to long-range order in the Peierls phase. We explain a previously observed feature at small momenta in terms of a hybridization of charge and phonon excitations. Tuning the system from a Peierls to a metallic phase with a nonzero Hubbard interaction suppresses the central peak, but a significant renormalization of the phonon dispersion remains. In contrast, the dispersion is only weakly modified in the Mott phase. We discuss finite-size effects, the relation to the dynamic charge structure factor, as well as additional sum rules and their implications. Finally, we reveal the existence of a discrete symmetry in a continuum field theory of the Holstein model, which is spontaneously broken in the Peierls phase.

PACS numbers: 71.10.Pm, 71.45.Lr, 71.30.+h, 71.38.-k

I. INTRODUCTION

Electron-phonon interaction plays a crucial role for the physics of materials [1], and gives rise to phenomena such as the Peierls instability [2], superconductivity, and polaron formation [3]. Recently, interest in electron-phonon interaction has also been boosted by experiments involving photo-induced phase transitions between insulating Peierls and metallic states [4], see Ref. [5] for a review.

The study of microscopic electron-phonon models has a long and rich history. Much of the recent progress on the theoretical side resulted from the development of exact numerical methods, most notably the density-matrix renormalization group [6–8], and quantum Monte Carlo (QMC) methods [9–15]. Whereas the case of a single electron (the polaron problem) can be solved to machine precision using a variational basis construction [16], finite band fillings are still a challenge. Here, we discuss one-dimensional (1D) models.

Of particular interest with regard to experiment is the calculation of spectral properties such as the electronic spectral function that may be compared to angular-resolved photoemission spectra. For the spinless Holstein model at half-filling, it reveals the opening of a Peierls gap for strong electron-phonon coupling [17–19], the experimentally observed shadow bands [20] arising from the new periodicity of the lattice [21], and soliton excitations [21]. The phonon spectral function and the dynamic charge structure factor—experimentally accessible via neutron scattering—reveal, for example, the softening of phonon excitations near the Peierls transition [19, 22, 23], and distinguish soft-mode behavior in the adiabatic regime from central-peak behavior in the nonadiabatic regime. For a single electron, the phonon spectrum can again be calculated to arbitrary precision [24]. The phonon spectral function and the renormalized phonon frequency of the spinless Holstein model were obtained with the projector-based renormalization method [17, 23, 25]. The electronic spectral function of

the Holstein-Hubbard model was calculated to characterize the metallic, Mott, and Peierls phases [26–28], and to study the impact of electron-phonon coupling on spin-charge separation [29, 30]. A more complete review of previous work can be found in Refs. [21, 28].

Here, we show that the CT-INT method, which was applied to a number of electron-phonon problems [15, 21, 28, 31–34], can also be used to calculate the phonon Green function, and thereby the phonon spectral function. The method is free of a Trotter error, and does not require a cutoff for the phonon Hilbert space. We use it to calculate the phonon spectral function of the half-filled Holstein-Hubbard model. The results are discussed in the context of previous work on these and other models, and additional insights are provided with the help of the random phase approximation and field theory.

The paper is organized as follows. In Sec. II we define the model. In Sec. III we discuss the method. Our results are presented in Sec. IV, followed by a discussion in Sec. V. Section VI contains our conclusions, and the Appendix discusses the relation between charge and phonon spectra, sum rules, and their implications.

II. MODEL

We consider the Holstein-Hubbard model

$$\hat{H} = -t \sum_{i\sigma} \left(\hat{c}_{i\sigma}^\dagger \hat{c}_{i+1\sigma} + \text{H.c.} \right) + U \sum_i \hat{n}_{i\uparrow} \hat{n}_{i\downarrow} \quad (1) \\ + \sum_i \left(\frac{1}{2M} \hat{P}_i^2 + \frac{K}{2} \hat{Q}_i^2 \right) - g \sum_i \hat{Q}_i \hat{\rho}_i.$$

The first term describes the hopping of electrons between neighboring lattice sites with amplitude t . The second term captures the repulsion between electrons at the same lattice site; for $U = 0$, Hamiltonian (1) becomes the spinful Holstein model [35]. The lattice is described in the harmonic approximation, with the displacement

(momentum) at site i given by \hat{Q}_i (\hat{P}_i). The bare optical phonon frequency is $\omega_0 = \sqrt{K/M}$. The electron-phonon interaction is of the density-displacement type, with $\hat{\rho}_i = \hat{n}_i - 1$, $\hat{n}_i = \sum_{\sigma} \hat{n}_{i\sigma}$, and $\hat{n}_{i\sigma} = \hat{c}_{i\sigma}^{\dagger} \hat{c}_{i\sigma}$. The dimensionless ratio $\lambda = g^2/(4Kt)$ is a useful measure of the electron-phonon coupling strength.

We studied Eq. (1) at half-filling, corresponding to $\langle \hat{n}_i \rangle = 1$, on chains with L sites and with periodic boundary conditions. We use t as the unit of energy, and set the lattice constant, M , and \hbar to one.

The Holstein-Hubbard model captures the Peierls transition driven by strong electron-phonon coupling, the Mott physics related to strong electron-electron interaction, and the competition between these two phenomena when $U \sim \lambda$ [26, 36–39]. Although some open questions remain regarding the phase diagram and the low-energy physics, the prevailing picture is that the model supports an intermediate metallic phase with a spin gap but gapless density fluctuations [28, 39], which is adiabatically connected to the metallic phase of the spinful Holstein model ($U = 0$) [8]. The metallic behavior for $\lambda < \lambda_c(U, \omega_0)$ is the result of quantum lattice fluctuations that destroy the long-range Peierls order. Its extent therefore depends on the phonon frequency: For $\omega_0 = 0$ a Peierls state exists as soon as $4\lambda t > U$, whereas for $\omega_0 = \infty$ a Peierls state is completely absent from the phase diagram [36–39]. In the classical limit and for half-filling, the charge order in the Peierls phase corresponds to spin-singlet pairs of electrons (singlet bipolarons) residing on every other lattice site.

We are not aware of any previous results for the phonon spectral function of the 1D Holstein-Hubbard model. The phonon spectrum of the 1D, half-filled spinless Holstein model was studied in Refs. [17, 19, 22, 23, 25]. Numerical results were obtained using exact diagonalization (restricted to small cluster sizes) [19], cluster perturbation theory (with artifacts related to the inherent translation symmetry breaking) [19], and QMC (restricted in cluster size and temperature, and with a Trotter error) [22]. Regarding analytical work, the projector-based renormalization group approach [17, 23, 25] provides the most comprehensive results. For $\omega_0 < t$, the renormalization of the phonon spectrum at large q was studied by means of the dynamic charge structure factor [21, 28]. A general feature of Holstein models is that for $\lambda = 0$, the phonon dispersion $\omega_q = \omega_0$ is trivial. However, for nonzero couplings, a renormalization takes place and $\omega_q \mapsto \tilde{\omega}_q$. For the spinless Holstein model, $\tilde{\omega}_q$ has been calculated in Refs. [17, 23].

III. METHOD

The CT-INT QMC method permits one to simulate rather general fermionic actions (including retarded and nonlocal interactions) [40]. Exploiting the fact that the phonon degrees of freedom can be integrated out exactly to obtain a fermionic action [15, 41], it was applied to a

number of different electron-phonon problems [15, 21, 28, 31–34]. The method relies on the imaginary-time path-integral formulation of the partition function, which is calculated using a weak-coupling perturbation expansion [15]. A strong-coupling formulation also exists, but is less suited for lattice problems [42].

For the model (1), the path-integral representation of the partition function takes the form

$$Z = \int \mathcal{D}(\bar{c}, c) e^{-S_0[\bar{c}, c]} - S_1[\bar{c}, c] \int \mathcal{D}(q) e^{-S_{\text{ep}}[\bar{c}, c, q]}, \quad (2)$$

where we used the coherent-state representation $\hat{c}_{i\sigma}|c\rangle = c_{i\sigma}|c\rangle$ with Grassmann variables $c_{i\sigma}$ for the fermions, and the real-space representation $\hat{Q}_i|q\rangle = q_i|q\rangle$ for the phonons. We split the action into the free-fermion part S_0 , the Hubbard interaction S_1 , and the remainder S_{ep} containing the free-phonon part as well as the coupling of the displacement fields to the electrons, given by

$$S_{\text{ep}} = \int_0^{\beta} d\tau \sum_i \left\{ \frac{M}{2} \dot{q}_i^2(\tau) + \frac{K}{2} q_i^2(\tau) - g q_i(\tau) \rho_i(\tau) \right\}. \quad (3)$$

Integration over the fields q in Eq. (2) leads to an effective fermionic action S_2 that can be simulated with the CT-INT method in the same way as fermionic models [15].

Previous applications of the CT-INT method were restricted to correlation functions of fermionic operators. By using a generating functional with source fields that couple to the lattice displacement fields, we can derive an estimator for the phonon propagator $D_{ij}(\tau)$ in terms of the time-displaced charge correlation function. Explicitly, to measure the phonon propagator

$$D_{ij}(\tau) = \langle q_i(\tau) q_j(0) \rangle, \quad (4)$$

we add a source term $S^{\eta} = -\int d\tau \sum_i \eta_i(\tau) q_i(\tau)$ to S_{ep} , where $\eta_i(\tau)$ is a real field. After integrating out the displacement fields, we arrive at an effective action describing the electron-phonon interaction,

$$S_2^{\eta} = -\frac{g^2}{2} \iint_0^{\beta} d\tau d\tau' \sum_i [\rho_i(\tau) + g^{-1} \eta_i(\tau)] \times D^0(\tau - \tau') [\rho_i(\tau') + g^{-1} \eta_i(\tau')]. \quad (5)$$

The appearance of the free phonon propagator

$$D^0(\tau) = \frac{1}{2M\omega_0} \frac{\cosh[\omega_0(\beta/2 - |\tau|)]}{\sinh[\omega_0\beta/2]}, \quad (6)$$

defined for $-\beta \leq \tau \leq \beta$, leads to a retarded interaction in imaginary time. The interacting propagator $D_{ij}(\tau)$ can be obtained from Eq. (5) via a functional derivative with respect to $\eta_i(\tau)$ in the limit $\eta \rightarrow 0$. The result,

$$D_{ij}(\tau) = D^0(\tau) \delta_{ij} + g^2 \iint_0^{\beta} d\tau_1 d\tau_2 D^0(\tau_1 - \tau) \times D^0(\tau_2) \langle \rho_i(\tau_1) \rho_j(\tau_2) \rangle, \quad (7)$$

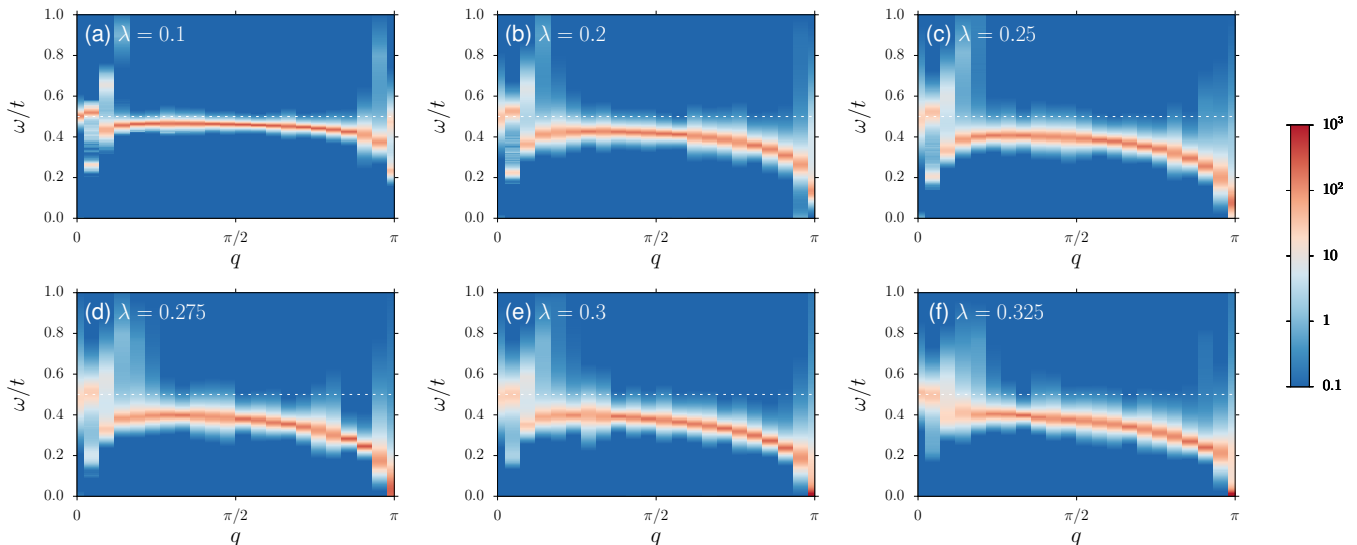


FIG. 1. (Color online) Phonon spectral function $B(q, \omega)$ of the spinful Holstein model. Dashed lines correspond to $\omega_0 = 0.5t$. Here, $U = 0$, and $\beta t = L = 42$. The Peierls transition occurs at $\lambda_c \approx 0.25$ [37, 38]. Color scheme based on Ref. [43].

is the sum of the free propagator and an interaction term that involves the time-displaced charge correlation function via a double convolution with $D^0(\tau)$. The charge correlation function can be accurately measured with the CT-INT method. Equation (7) has previously been derived for the Anderson-Holstein impurity model [44].

We evaluated Eq. (7) for each bin average of $\langle n_i(\tau)n_j(0) \rangle$, and used a binning analysis to obtain reliable statistical errors. To minimize systematic errors in the numerical integration, we carried out one of the integrals in Eq. (7) analytically by exploiting the periodicity of $D^0(\tau)$ and $\langle n_i(\tau)n_j(0) \rangle$. Measurements were made on an equidistant grid on the imaginary time axis with $\Delta\tau t = 0.1$. From $D_{ij}(\tau)$ we obtained the phonon spectral function (we define $\Delta_{nm} = E_n - E_m$)

$$B(q, \omega) = \frac{1}{Z} \sum_{n,m} |\langle m | \hat{Q}_q | n \rangle|^2 e^{-\beta E_m} \delta(\omega - \Delta_{nm}) \quad (8)$$

by carrying out a Fourier transformation and using the stochastic maximum entropy method [45] for the analytic continuation. The use of $\rho_i(\tau)$ instead of $n_i(\tau)$ in Eq. (7) amounts to subtracting the $T = 0$ static contribution to $B(q = 0, \omega)$. Our results obey the sum rule $\int_0^\infty d\omega B(q, \omega)(1 + e^{-\beta\omega}) = D(q, \tau = 0)$. Additional sum rules are discussed in the appendix.

IV. NUMERICAL RESULTS

We first consider the spinful Holstein model [Eq. (1) with $U = 0$] with $\omega_0 = 0.5t$, which exhibits a Peierls metal-insulator transition at $\lambda_c \approx 0.25$ [37, 38]. Figure 1 shows the phonon spectral function $B(q, \omega)$ for different

values of λ . The system size and temperature were chosen as $L = \beta t = 42$ (see also Sec. V).

For a weak coupling $\lambda = 0.1$, Fig. 1(a) reveals that the bare phonon mode at $\omega_q = \omega_0$ is renormalized near $q = 0$ and $q = \pi$, but largely unaffected at intermediate q . The small- q feature will be explained as a hybridization effect in Sec. V. For a stronger coupling $\lambda = 0.2$, shown in Fig. 1(b), the renormalization of the phonon mode is significantly more pronounced, and we observe a partial softening near $q = \pi = 2k_F$, which is a precursor of the Peierls transition. Upon increasing λ further, the phonon spectrum becomes gapless close to $\lambda_c = 0.25$. Beyond λ_c , the results in Figs. 1(d)–1(f) are consistent (see below) with the emergence of a central ($\omega = 0$) peak at $q = \pi$, and a second peak at $\omega > 0$. The central peak carries substantial spectral weight (which diverges with system size) and reflects the long-range lattice order with modulation $q = 2k_F = \pi$. The phonon dispersion throughout the Brillouin zone appears to be most pronounced for $\lambda \approx \lambda_c$, and becomes flatter in the Peierls phase.

To understand the evolution of $B(q, \omega)$ at the ordering wavevector $q = \pi$ in more detail, we show in Fig. 2 the spectrum $B(\pi, \omega)$ for the same parameters as in Fig. 1. Except for $\lambda = 0.275$, we observe two separate low-energy peaks in the phonon spectrum, although they are difficult to discern in the density plots of Fig. 1. Starting at weak coupling $\lambda = 0.1$, there is a peak at $\omega \approx 0.2t$ (corresponding to the finite-size charge gap in the dynamic charge structure factor at $q = \pi$, which scales as $1/L$), and a peak close to the bare phonon frequency $\omega = \omega_0 = 0.5t$. With increasing λ , both peaks move toward smaller ω . For the system size used, the spectrum becomes gapless close to the critical coupling $\lambda_c \approx 0.25$, coinciding with the appearance of the central peak. Figures 2(e) and 2(f) reveal that a second peak emerges that becomes harder

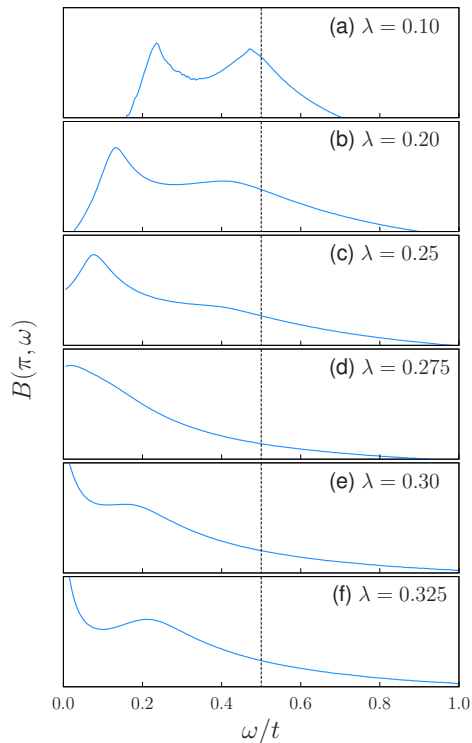


FIG. 2. (Color online) Phonon spectral function $B(q, \omega)$ at $q = \pi$ for the same parameters as in Fig. 1. The dashed vertical lines indicate $\omega_0 = 0.5t$. As in Fig. 1, we use a logarithmic scale and a plot range $[0.1, 10^3]$.

with increasing λ but has small spectral weight compared to the central peak.

It is also interesting to consider the impact of Coulomb repulsion in the framework of the Holstein-Hubbard model. In Fig. 3(a) we show the phonon spectral function for $\lambda = 0.3$ and $U = t$, which should be compared to the results of Fig. 1(e). Quite remarkably, we find a comparable renormalization of the bare phonon mode, but no central peak. The absence of the latter is expected since $U = t$ is sufficient to drive the system from the Peierls into the intermediate metallic phase, cf. Fig. 8(a) in Ref. [37]. On the other hand, the renormalization of the phonon mode is much stronger than expected based on a simple effective Hubbard model with interaction $U_{\text{eff}} = U - 4t\lambda$, which is justified for sufficiently large ω_0/t . For the parameters of Fig. 3(a), we have $U_{\text{eff}} = -0.2t$. However, the phonon spectrum is renormalized more strongly than in Fig. 1(a), where $\lambda = 0.1$ and $U_{\text{eff}} = -0.4t$, suggesting that not only the effective interaction but also the bare electron-phonon coupling determines the phonon renormalization. Finally, for $U = 2t$ [Fig. 3(b)], corresponding to the Mott phase [37], the renormalization of the phonon mode is significantly weaker, and the phonon spectrum resembles quite closely the weak-coupling results shown in Fig. 1(a).

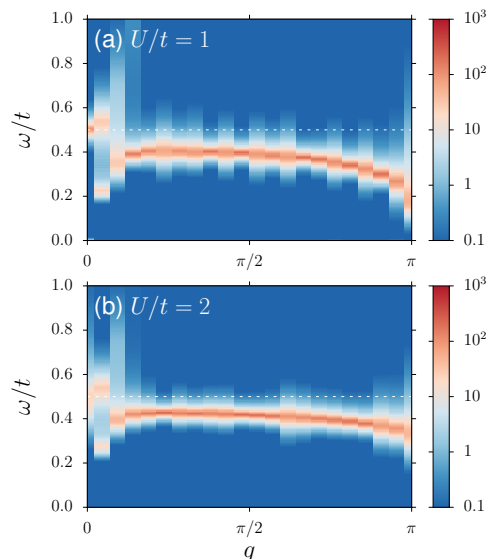


FIG. 3. (Color online) Phonon spectral function $B(q, \omega)$ of the Holstein-Hubbard model. The dashed line corresponds to $\omega_0 = 0.5t$. Here, $\lambda = 0.3$, and $\beta t = L = 42$.

V. DISCUSSION

In this section, we relate our numerical results to previous work and to theoretical expectations. Additionally, we provide an explanation of the small- q feature observed in the metallic phase, and show how the discrete symmetry spontaneously broken at the Peierls transition can be captured in a continuum field theory.

A. Relation to the charge structure factor

As illustrated by the exact relation (7), the phonon Green function and the time-displaced charge correlation function are related by a convolution. Consequently, the phonon spectral function $B(q, \omega)$ and the dynamic charge structure factor

$$N(q, \omega) = \frac{1}{Z} \sum_{n,m} |\langle m | \hat{\rho}_q | n \rangle|^2 e^{-\beta E_m} \delta(\omega - \Delta_{nm}), \quad (9)$$

with $\hat{\rho}_q = L^{-1/2} \sum_r e^{iqr} \hat{\rho}_r$, contain in principle the same information, although the spectral weights may differ by orders of magnitude. In particular, as discussed in more detail in the Appendix, the dynamic charge structure factor also reveals the renormalized phonon excitations [21, 28, 31], and the phonon spectral function also contains signatures of the particle-hole continuum.

Importantly, for values of q where the bare phonon mode and the particle-hole continuum overlap, the renormalized phonon mode $\tilde{\omega}_q$ will be damped, in contrast to the δ -function contribution suggested by the approximation for $B(q, \omega)$ given in Eq. (5) of Ref. [23]. For intermediate phonon frequencies $\omega_0 \approx t$, no clear separation

exists between the phonon mode and particle-hole excitations. Finally, for $\omega_0 \gg t$ (that is, larger than the bare bandwidth $4t$ of the particle-hole continuum), or deep in the Peierls phase where the lower edge of the particle-hole continuum lies above $\tilde{\omega}_q$, we expect the phonon mode to remain a separate and well-defined excitation near $q = 2k_F$, as suggested by Figs. 3(b) and 2(a) in Ref. [23], respectively.

An important corollary of the relation between $B(q, \omega)$ and $N(q, \omega)$ concerns the shape of the spectrum in the vicinity of $q = \pi$. In the Peierls phase, the size of the unit cell (Brillouin zone) doubles (halves). Although a perfect symmetry (extending to the spectral weights of excitations) between $q = 0$ and $q = \pi$ is only achieved in the limit $\lambda \rightarrow \infty$, this doubling implies that the renormalized phonon frequency $\tilde{\omega}_q$ cannot extrapolate to zero at $q = \pi$ for $\lambda > \lambda_c$. Such a gapless mode would necessarily have a counterpart near $q = 0$, and also in $N(q, \omega)$. However, gapless, long-wavelength particle-hole excitations are not compatible with an insulating Peierls state. We will see below that a simple low-energy theory instead suggests a gapped renormalized phonon mode and an isolated central peak at $q = \pi$. This picture is consistent with our numerical results. On the other hand, we attribute the apparent existence of a gapless mode near $q = \pi$ in results for the spinless Holstein model [21] to a failure to resolve the expected two-peak structure in the dynamic charge structure factor.

B. Origin of the small- q feature

The coupling between the bare phonon mode and the particle-hole excitations of $N(q, \omega)$ [see Fig. 4(a)] via the electron-phonon interaction provides an explanation of the small- q feature visible in Fig. 1(a), as well as in the renormalized phonon frequency $\tilde{\omega}_q$ in Refs. [17, 25]. In the analytical results of Refs. [17, 25], this feature occurs at a nonzero q and is quite sharp in momentum space, making it difficult to resolve fully in our finite-size data and explaining its absence in previous exact diagonalization results for small clusters [19].

Here, we explain this feature in terms of the hybridization between the bare phonon frequency $\omega_q = \omega_0$ and particle-hole excitations that—in one dimension—have the linear dispersion $\omega = v_F q$ for small q , see Fig. 4(a). The hybridization is captured by the random phase approximation for the phonon propagator,

$$D^{-1}(q, i\Omega_n) = [D^0(i\Omega_n)]^{-1} + \lambda^2 \chi^0(q, i\Omega_n), \quad (10)$$

where Ω_n is a bosonic Matsubara frequency, and $\chi^0(q, i\Omega_n)$ is the noninteracting charge susceptibility. Taking λ as a free parameter to match the numerical results, we find a hybridization at the intersection point of the free phonon dispersion and the free particle-hole excitations, as well as a gapless linear mode below the bare dispersion that corresponds to long-wavelength charge

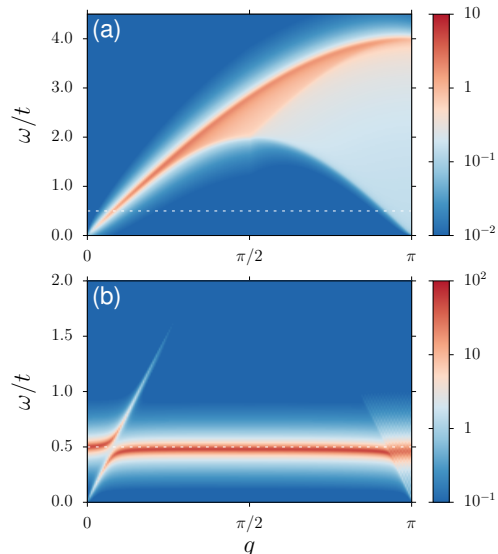


FIG. 4. (Color online) (a) Dynamic charge structure factor of the noninteracting system ($\lambda = U = 0$). (b) Phonon spectral function from Eq. (10) for $\lambda = 0.2$. The dashed lines indicate $\omega_0 = 0.5t$. Here, $T = 0$, and $L = 402$.

fluctuations. While the CT-INT results in, for example, Fig. 1(a), do not fully resolve the hybridization, the agreement is satisfactory. Note that the random phase approximation does not take into account any phonon softening related to charge order, or the renormalization of v_F by interactions. The hybridization of charge and phonon modes at small q also follows from a Tomonaga-Luttinger model [46].

In accordance with the analytical results of Refs. [17, 25], a hybridization of the phonon mode with the particle-hole continuum is also visible near $q = \pi$, and gives rise to damping of the phonon excitations. The above explanation suggests that the small- q feature is absent deep in the insulating Peierls phase, because the latter does not have low-energy excitations near $q = 0$. Accordingly, a suppression of the hybridization feature with increasing λ is visible in Fig. 1. Finally, within the random phase approximation, the hybridization does not explain the observed hardening of the phonon mode near the zone boundary for $\omega_0 = 4t$ [19].

C. Finite-size effects

Although our system size of $L = 42$ is significantly larger than in previous work, it is important to separate finite-size effects from generic features.

The most notable finite-size artifact in our results is the charge gap at $q = \pi$ in the dynamic charge structure factor and (for $\lambda > 0$) also in the phonon spectral function. In the noninteracting case, this gap scales as $1/L$. While it is negligibly small in Fig. 4(a) ($L = 402$), it is about $0.3t$ for the system size $L = 42$ used in our

simulations. The results for the phonon spectral function in Fig. 2 reveal that with increasing λ , the charge gap is reduced. At the critical point, the central peak at $\omega = 0$ appears. The closing of the finite-size charge gap almost exactly at the critical coupling λ_c is not expected to be generic, but to depend on system size and parameters.

While a charge gap is expected in $B(\pi, \omega)$ in the Peierls phase even in the thermodynamic limit, both $B(q, \omega)$ and $N(q, \omega)$ are gapless at $q = \pi$ throughout the metallic phase for $L \rightarrow \infty$ [23]. In the insulating Peierls phase, the central peak at $\omega = 0$ is separated from excitations with $\omega > 0$ by the interaction-generated charge gap. Importantly, the lower edge of the particle-hole continuum in the metallic phase corresponds to a branch cut (similar to other excitations of 1D systems) with finite spectral weight, whereas the weight of the central peak at $\omega = 0$ in the Peierls phase diverges in the thermodynamic limit. Finite-size effects on the phonon spectrum of a spin-Peierls model have been discussed in Ref. [47].

To avoid spurious finite-size effects, the system size should be large enough to have a noninteracting charge gap smaller than the bare phonon frequency. Otherwise, there is no coupling between the bare mode and the particle-hole continuum, which is not generic for the adiabatic regime. In the latter, and more generally for any $\omega_0 < 4t$, the bare phonon mode lies on top of the noninteracting particle-hole continuum in extended regions of the Brillouin zone. A nonzero electron-phonon coupling then gives rise to a mixing of these excitations, leading to renormalization and a finite lifetime of phonon excitations. In this sense, Eq. (5) in Ref. [23] should be regarded as an approximate result because it suggests the existence of phonon excitations with infinite lifetime described by $\delta(\omega - \tilde{\omega}_q)$.

D. Soft-mode versus central-peak behavior

Peierls transitions are often classified as either soft-mode or central-peak transitions. In terms of the coupling λ (rather than temperature, as appropriate for experiments on quasi-1D systems), a 1D soft-mode transition involving a single phonon mode is characterized by a softening $\omega_{2k_F} \rightarrow 0$ for $\lambda < \lambda_c$, a completely soft mode $\omega_{2k_F} = 0$ at $\lambda = \lambda_c$, and a subsequent hardening (i.e., $\omega_{2k_F} > 0$) in the Peierls phase with an additional central peak at $\omega = 0$ reflecting the long-range lattice order. In contrast, for a central-peak transition, ω_{2k_F} stays nonzero or even hardens across the transition, and a central peak appears at the critical point and persists for $\lambda > \lambda_c$.

The above simple picture is modified in several ways. (i) Because of the relation to the charge structure factor, $B(q, \omega)$ in general has a continuum of excitations. Although the spectra shown here for the adiabatic regime are dominated by a few peaks, the particle-hole continuum has substantial spectral weight for $\omega_0 > t$ [19, 23]. (ii) In the thermodynamic limit, $B(q, \omega)$ has soft (i.e., gapless) excitations in the metallic phase corresponding

to the gapless particle-hole continuum at $q = \pi$. (iii) In the Peierls phase, the renormalized phonon mode (which has a finite energy for $\lambda > \lambda_c$) has very small spectral weight compared to the divergent central peak, which may make its identification difficult for both numerical simulations and experiments. Similar behavior has been reported for a spin-Peierls model in Ref. [47]; in particular, it was pointed out that the two peaks in $B(q, \pi)$ are only visible on large enough system sizes. Finally, it is not clear if the hardening of ω_{2k_F} in the Peierls phase can be clearly distinguished from the opening of the gap in the particle-hole continuum in the vicinity of λ_c .

Keeping in mind these complications, our numerical results in Figs. 1 and 2 are nevertheless compatible with a soft mode transition. The dispersive feature that exists throughout the Brillouin zone and emerges from the bare phonon mode $\omega_q = \omega_0$ upon turning on the electron-phonon interaction can be identified with the renormalized phonon frequency $\tilde{\omega}_q$. We observe that $\tilde{\omega}_q$ softens near $q = \pi$ as $\lambda \rightarrow \lambda_c$, and hardens again in the Peierls phase. However, due to limitations in system size and spectral resolution, we are unable to unambiguously demonstrate the existence of a true soft mode at λ_c .

Let us briefly discuss relevant previous works on this issue. In Refs. [17, 23, 25], the renormalized phonon frequency $\tilde{\omega}_q$ of the spinless Holstein model was found to soften at the critical point, and harden again in the Peierls phase. This behavior is consistent with a soft-mode transition, but the results for the phonon spectral function in Fig. 2 of Ref. [23] do not seem to show a central peak related to long-range order, in contrast to numerical results [19]. A softening is also visible in exact diagonalization results for small clusters in Ref. [19]. Based on QMC simulations and fits of the phonon propagator to a simple two-mode form, a softening (hardening) in the metallic (insulating) phase was suggested in Ref. [22]. Although we can reproduce these results, it is not clear how reliable such fits are given the large ratio of spectral weights between the central peak and the phonon peak. Moreover, we find that the minimum of the fitted phonon frequency does not give the correct critical value λ_c in the adiabatic regime ($\omega_0 = 0.1t$). Finally, the phonon softening and ensuing hardening observed in Migdal-Eliashberg theory [48] and in approximate solutions of the Holstein model [49] for any band filling appear to be a consequence of the breakdown of the adiabatic approximation. A soft phonon mode seems to be always linked with a lattice instability (phase transition), which requires a commensurate band filling.

E. Field-theory description

The observation of a Peierls transition implies the existence of a Z_2 symmetry which, in one dimension, can be spontaneously broken at zero temperature and would account for the observed central peak. Here we provide a minimal continuum theory that reveals such a Z_2 symme-

try for the Holstein model. For simplicity, we consider spinless fermions and assume an arbitrary value of the Fermi wave vector k_F .

Near $\pm k_F$, the electronic degrees of freedom can be described by a linear dispersion, leading to the Dirac form

$$\hat{H}_e = v_F \sum_k k \Psi_k^\dagger \sigma_z \Psi_k, \quad (11)$$

where $\Psi_k^\dagger = (\hat{L}_k^\dagger, \hat{R}_k^\dagger)$ is a spinor of creation operators for left and right moving fermions, respectively, and σ_z is the usual Pauli matrix. \hat{H}_e has a $U_{S_z}(1)$ symmetry related to the pseudospin $\hat{S}_z = \frac{1}{2} \sum_k \Psi_k^\dagger \sigma_z \Psi_k$; we have $\hat{U}_\theta^{-1} \Psi_k \hat{U}_\theta = U_\theta \Psi_k$ with $\hat{U}_\theta = e^{i\theta \hat{S}_z}$ and $U_\theta = e^{i(\theta/2)\sigma_z}$.

The free phonon part can be written as

$$\hat{H}_p = \sum_k \omega_k \hat{\alpha}_k^\dagger \hat{\alpha}_k \quad (12)$$

with $\omega_k = \omega_0$ for optical phonons.

In the framework of bosonization, the Peierls transition arises from phonon-mediated single-particle backscattering described by (see Appendix B of Ref. [31])

$$\hat{H}_I = \frac{\tilde{g}}{\sqrt{L}} \sum_{k,q} \left[\hat{R}_k^\dagger \hat{L}_{k-q} \left(\hat{\alpha}_{-2k_F-q}^\dagger + \hat{\alpha}_{2k_F+q} \right) + \hat{L}_{k-q}^\dagger \hat{R}_k \left(\hat{\alpha}_{2k_F+q}^\dagger + \hat{\alpha}_{-2k_F-q} \right) \right]. \quad (13)$$

To derive a low-energy theory, we only consider small momenta $|q| \ll 2k_F$. Consequently, for our purposes, $\hat{\alpha}_{-2k_F-q}^\dagger$ and $\hat{\alpha}_{2k_F+q}$ may be regarded as independent bosonic modes [50]. With $\alpha_q^\dagger = (\hat{\alpha}_{-2k_F-q}^\dagger, \hat{\alpha}_{2k_F+q}^\dagger)$ the phonon Hamiltonian can be written as

$$\hat{H}_p = \sum_q \alpha_q^\dagger [\omega_+(q) + \omega_-(q)\sigma_z] \alpha_q, \quad (14)$$

where $\omega_\pm(q) = (\omega_{-2k_F-q} \pm \omega_{2k_F+q})/2$. Under the above assumption of two independent modes, \hat{H}_p has two $U(1)$ symmetries generated by the conservation of the total phonon number $\hat{N} = \sum_q \alpha_q^\dagger \alpha_q$, and of $\hat{N}_z = \sum_q \alpha_q^\dagger \sigma_z \alpha_q$, denoted as $U_N(1)$ and $U_{N_z}(1)$, respectively.

The electron-phonon interaction term (13) breaks the full $U_N(1) \times U_{N_z}(1) \times U_{S_z}(1)$ of the free Hamiltonian (in particular, the number of phonons is not conserved). However, under a combined transformation $\hat{U}_{\phi,\theta} = e^{i\phi \hat{N}_z} e^{i\theta \hat{S}_z}$ the interaction term transforms as

$$\hat{U}_{\phi,\theta}^{-1} \hat{H}_I \hat{U}_{\phi,\theta} = \frac{\tilde{g}}{\sqrt{L}} \sum_{k,q} \Psi_k^\dagger U_\theta^\dagger \sigma_- U_\theta \Psi_{k-q} e^{i\phi} \times \left(\hat{\alpha}_{-2k_F-q}^\dagger + \hat{\alpha}_{2k_F+q} \right) + \text{H.c.}, \quad (15)$$

where $\sigma_\pm = \frac{1}{2}(\sigma_x \pm i\sigma_y)$. Since $U_\theta^\dagger \sigma_- U_\theta = e^{i\theta} \sigma_-$, setting $\theta = -\phi$ shows that $\hat{S}_z - \hat{N}_z$ is a generator of a $U_{S_z-N_z}(1)$ symmetry of the full Hamiltonian $\hat{H}_e + \hat{H}_p + \hat{H}_I$. On the other hand the interaction term reduces the

$U_N(1)$ symmetry to a discrete Z_2 symmetry. Therefore, the symmetry of the full Hamiltonian is $U_{S_z-N_z}(1) \times Z_2$.

As mentioned previously, the $U_{S_z-N_z}(1) \times Z_2$ symmetry can explain the existence of a Peierls state with long-range order at $T = 0$. The $U_{S_z-N_z}(1)$ symmetry accounts for a combined charge and phonon mode, whereas the Z_2 symmetry, if broken at $T = 0$, gives rise to the central peak feature. Within our continuum field-theory description, commensurate band fillings cannot be unambiguously defined. Nevertheless, the reduction of the $U_N(1)$ symmetry to Z_2 accounts for the expected pinning of the charge-density wave for commensurate band fillings [51]. The $U_{S_z-N_z}(1)$ symmetry is reminiscent of the $U(1)$ Gross-Neveu theory with one bosonic mode and two fermion flavors [52] that describes, for example, the transition from a Dirac semimetal to a Kekule ordered state in two dimensions [53].

VI. CONCLUSIONS

We showed that the phonon spectral function of electron-phonon models can be calculated using the CT-INT QMC method with the help of a generating functional. The same idea can be used to measure other correlation functions and observables, and for other models, which further extends the usefulness and versatility of the CT-INT method.

Our results for the 1D Holstein-Hubbard model are consistent with a soft-mode Peierls transition in the adiabatic regime, characterized by a softening of the $q = 2k_F$ phonon excitations, a gapless mode at the critical point, and a subsequent hardening of the phonon mode in the Peierls phase. However, this simple picture is complicated by finite-size effects, and by the mixing of phonon and charge excitations mediated by the electron-phonon interaction. We explained a small- q anomaly of the metallic phase, previously observed for the spinless Holstein model, in terms of a hybridization of the bare phonon mode and the particle-hole continuum. Overall, our results for the spinful Holstein model are very similar to previous results for the spinless Holstein model.

For a Hubbard repulsion large enough to yield a metallic state, we observed a suppression of the central peak related to long-range order, but a significant remaining renormalization of the phonon mode that only disappears in the Mott phase for even larger Hubbard interaction.

Finally, we provided a unified picture of current and previous work, and showed how the discrete symmetry spontaneously broken in the Peierls phase can be captured in a continuum field theory.

ACKNOWLEDGMENTS

We acknowledge access to the Jülich Supercomputing Centre, and financial support from the DFG Grants No.

AS120/10-1 and No. Ho 4489/3-1 (FOR 1807). We further thank J. Bhaseen, F. Goth, I. Herbut, J. Hofmann, F. Parisen Toldin, and G. Wellein for helpful discussions.

Appendix: Exact relation between phonon and charge spectra

For the Holstein model, the phonon spectral function $B(q, \omega)$ and the dynamic charge structure factor $N(q, \omega)$ in principle contain the same information. Here, starting from Eq. (7), we derive an exact relation between the spectral functions as well as additional sum rules, and discuss the implications.

1. Analytic properties of the spectral functions

To simplify the notation, we define $\bar{B}(q, \omega) = (1 - e^{-\beta\omega})B(q, \omega)$ and $\bar{N}(q, \omega) = (1 - e^{-\beta\omega})N(q, \omega)$. The phonon spectral function $\bar{B}(q, \omega)$ can be obtained from the Lehmann representation of the phonon propagator

$$D(q, z) = - \int_{-\infty}^{\infty} d\omega \frac{\bar{B}(q, \omega)}{z - \omega} \quad (\text{A.1})$$

by analyzing its pole structure in the complex-frequency plane. For simplicity, we restrict our considerations to finite Hilbert spaces, where $D(q, z)$ has only simple poles on the real axis [54] determined by the exact relation

$$D(q, z) = D^0(z) + g^2 D^0(z)^2 \chi(q, z). \quad (\text{A.2})$$

The term $\sim g^2$ in Eq. (A.2) gives rise to a product of poles arising from the free phonon propagator $D^0(z) = M^{-1}(\omega_0^2 - z^2)^{-1}$ and the charge susceptibility

$$\chi(q, z) = \langle \rho_q(z) \rho_{-q} \rangle = - \int_{-\infty}^{\infty} d\omega \frac{\bar{N}(q, \omega)}{z - \omega}. \quad (\text{A.3})$$

A partial-fraction decomposition and comparison of the pole structure of the two sides of Eq. (A.2) gives

$$\bar{B}(q, \omega) = \bar{B}^0(q, \omega) + g^2 D^0(\omega)^2 \bar{N}(q, \omega) + \bar{B}^1(q, \omega). \quad (\text{A.4})$$

For $g = 0$, the phonon spectral function is given by

$$\bar{B}^0(q, \omega) = \frac{1}{2M\omega_0} [\delta(\omega - \omega_0) - \delta(\omega + \omega_0)], \quad (\text{A.5})$$

which describes excitations at the bare phonon frequency $\omega = \pm\omega_0$. Any finite electron-phonon coupling leads to the appearance of two additional terms in Eq. (A.4): The first contains the whole charge spectrum $\bar{N}(q, \omega)$ reweighted by the free phonon propagator, while

$$\begin{aligned} \bar{B}^1(q, \omega) = & -\frac{g^2}{\omega_0} [\delta(\omega - \omega_0) - \delta(\omega + \omega_0)] \\ & \times \mathcal{P} \int_0^{\infty} d\omega' \omega' D^0(\omega')^2 \bar{N}(q, \omega') \end{aligned} \quad (\text{A.6})$$

gives an additional contribution at $\omega = \pm\omega_0$. Here, \mathcal{P} denotes the principal value.

To derive Eq. (A.4), we used a partial-fraction decomposition, leading to poles of both first and second order. However, poles of second order are forbidden by the Lehmann representation (A.1). Therefore, their weights have to vanish, which (for $\omega_0 > 0$) leads to the sum rule

$$\mathcal{P} \int_0^{\infty} d\omega \frac{\omega}{\omega^2 - \omega_0^2} \bar{N}(q, \omega) = 0. \quad (\text{A.7})$$

From Eqs. (A.4) and (A.7), we obtain an equivalent sum rule for $\bar{B}(q, \omega)$,

$$\int_0^{\infty} d\omega \omega (\omega^2 - \omega_0^2) \bar{B}(q, \omega) = 0, \quad (\text{A.8})$$

which is just a combination of the first and third moment of $\bar{B}(q, \omega)$. In the same way, the absence of higher-order poles requires $\bar{N}(q, \omega = \pm\omega_0) = 0$.

For finite electron-phonon coupling, Eq. (A.2) can also be used to obtain the charge spectrum

$$\bar{N}(q, \omega) = \frac{M^2}{g^2} (\omega^2 - \omega_0^2)^2 \bar{B}(q, \omega) \quad (\text{A.9})$$

from the phonon spectral function. Here, contributions at $\omega = \pm\omega_0$ are removed from $\bar{N}(q, \omega)$ by the prefactor.

2. Implications for the spectral properties

According to Eqs. (A.4) and (A.9), $B(q, \omega)$ and $N(q, \omega)$ share the same spectral information, up to an additional contribution to $\bar{B}(q, \pm\omega_0)$ that consists of the free phonon spectrum $B^0(q, \omega)$ and a compensating term $B^1(q, \omega)$ due to finite interactions.

For $q = 0$, because of charge conservation, $N(q, \omega)$ only has a static contribution at $\omega = 0$. Thus, $B^1(q = 0, \omega) = 0$ and the full phonon spectrum is given by the free part at $\omega = \pm\omega_0$ and the static contribution to $N(q, \omega)$.

For $q \neq 0$, any finite electron-phonon coupling seems to shift the phonon dispersion away from $\omega = \pm\omega_0$. Exact diagonalization data for the spinless Holstein model [19] suggest that $B(q, \pm\omega_0)$ vanishes and therefore $B^0(q, \omega)$ and $B^1(q, \omega)$ compensate each other [55]. In general, for $q \neq 0$, both $B(q, \omega)$ and $N(q, \omega)$ contain signatures of the phonon dispersion as well as the particle-hole continuum, although the spectral weights may be very different.

The condition $B(q, \omega_0) \geq 0$ sets an upper bound to the integral in Eq. (A.6),

$$\mathcal{P} \int_0^{\infty} d\omega \frac{\omega}{(\omega^2 - \omega_0^2)^2} \bar{N}(q, \omega) \leq \frac{M}{2g^2}. \quad (\text{A.10})$$

For the integral to converge, $N(q, \omega)$ has to vanish when approaching ω_0 . Thus, a nonzero electron-phonon interaction splits the charge spectrum at $\omega = \omega_0$.

Further insight into the distribution of spectral weight can be obtained from the sum rules (A.7) and (A.8). We

restrict our discussion to $B(q, \omega)$, but the same arguments hold for $N(q, \omega)$. For $\omega > 0$, $B(q, \omega) \geq 0$ but the prefactor $(\omega^2 - \omega_0^2)$ changes sign at ω_0 . This sign change divides the frequency axis into regions $\omega < \omega_0$ and $\omega > \omega_0$, whose integrated spectral weights have to compensate each other in the sum rule [56]. Note that spectral weight at $\omega = 0$ and $\omega = \omega_0$ does not contribute to the sum rule, therefore the noninteracting phonon dispersion fulfills Eq. (A.8) trivially. By adiabatically switching on the electron-phonon coupling, the particle-hole continuum enters $B(q, \omega)$ and spectral weight has to be redis-

tributed to fulfill Eq. (A.8). For wave vectors such that the particle-hole continuum only enters one of the two regions, spectral weight has to appear in the other region. This can be most easily achieved by shifting the phonon dispersion. Both the hardening of the phonon dispersion for $\omega_0 \gg t$ [19, 23], and the hybridization with the particle-hole continuum as well as the phonon softening for $\omega_0 \ll t$, are consistent with the sum rule (A.8). Furthermore, in the Peierls phase, the charge gap (the lowest excitation at $q = \pi$) cannot become larger than ω_0 , as the central peak does not contribute to the sum rule (A.8).

-
- ¹ A. S. Alexandrov, ed., *Polarons in Advanced Materials* (Canopus Publishing and Springer Verlag GmbH, Bristol (UK), 2007).
- ² R. Peierls, *Surprises in Theoretical Physics* (Princeton University Press, New Jersey, 1979).
- ³ J. T. Devreese and A. S. Alexandrov, Rep. Prog. Phys. **72**, 066501 (2009).
- ⁴ M. Chollet, L. Guerin, N. Uchida, S. Fukaya, H. Shimoda, T. Ishikawa, K. Matsuda, T. Hasegawa, A. Ota, H. Yamochi, G. Saito, R. Tazaki, S.-i. Adachi, and S.-y. Koshihara, Science **307**, 86 (2005).
- ⁵ K. Yonemitsu and K. Nasu, Phys. Rep. **465**, 1 (2008).
- ⁶ U. Schollwöck, Rev. Mod. Phys. **77**, 259 (2005).
- ⁷ R. J. Bursill, R. H. McKenzie, and C. J. Hamer, Phys. Rev. Lett. **80**, 5607 (1998).
- ⁸ E. Jeckelmann, C. Zhang, and S. R. White, Phys. Rev. B **60**, 7950 (1999).
- ⁹ R. Blankenbecler, D. J. Scalapino, and R. L. Sugar, Phys. Rev. D **24**, 2278 (1981).
- ¹⁰ H. De Raedt and A. Lagendijk, Phys. Rev. Lett. **49**, 1522 (1982).
- ¹¹ E. Fradkin and J. E. Hirsch, Phys. Rev. B **27**, 1680 (1983).
- ¹² P. E. Kornilovitch, Phys. Rev. Lett. **81**, 5382 (1998).
- ¹³ N. V. Prokof'ev and B. V. Svistunov, Phys. Rev. Lett. **81**, 2514 (1998).
- ¹⁴ A. W. Sandvik and D. K. Campbell, Phys. Rev. Lett. **83**, 195 (1999).
- ¹⁵ F. F. Assaad and T. C. Lang, Phys. Rev. B **76**, 035116 (2007).
- ¹⁶ J. Bonča, S. A. Trugman, and I. Batistic, Phys. Rev. B **60**, 1633 (1999).
- ¹⁷ S. Sykora, A. Hübsch, K. W. Becker, G. Wellein, and H. Fehske, Phys. Rev. B **71**, 045112 (2005).
- ¹⁸ H. Zhao, C. Q. Wu, and H. Q. Lin, Phys. Rev. B **71**, 115201 (2005).
- ¹⁹ M. Hohenadler, G. Wellein, A. R. Bishop, A. Alvermann, and H. Fehske, Phys. Rev. B **73**, 245120 (2006).
- ²⁰ J. Voit, L. Perfetti, F. Zwick, H. Berger, G. Margaritondo, G. Grüner, H. Höchst, and M. Grioni, Science **290**, 501 (2000).
- ²¹ M. Hohenadler, H. Fehske, and F. F. Assaad, Phys. Rev. B **83**, 115105 (2011).
- ²² C. E. Creffield, G. Sangiovanni, and M. Capone, Eur. Phys. J. B **44**, 175 (2005).
- ²³ S. Sykora, A. Hübsch, and K. W. Becker, Europhys. Lett. **76**, 644 (2006).
- ²⁴ J. Loos, M. Hohenadler, A. Alvermann, and H. Fehske, J. Phys.: Condens. Matter **18**, 7299 (2006).
- ²⁵ S. Sykora, A. Hübsch, and K. W. Becker, Eur. Phys. J. B **51**, 181 (2006).
- ²⁶ H. Fehske, G. Wellein, G. Hager, A. Weiße, and A. R. Bishop, Phys. Rev. B **69**, 165115 (2004).
- ²⁷ A. Payeur and D. Sénéchal, Phys. Rev. B **83**, 033104 (2011).
- ²⁸ M. Hohenadler and F. F. Assaad, Phys. Rev. B **87**, 075149 (2013).
- ²⁹ W. Q. Ning, H. Zhao, C. Q. Wu, and H. Q. Lin, Phys. Rev. Lett. **96**, 156402 (2006).
- ³⁰ H. Matsueda, T. Tohyama, and S. Maekawa, Phys. Rev. B **74**, 241103 (2006).
- ³¹ F. F. Assaad, Phys. Rev. B **78**, 155124 (2008).
- ³² M. Hohenadler, F. F. Assaad, and H. Fehske, Phys. Rev. Lett. **109**, 116407 (2012).
- ³³ M. Hohenadler, Phys. Rev. B **88**, 064303 (2013).
- ³⁴ M. Weber, F. F. Assaad, and M. Hohenadler, Phys. Rev. B **91**, 245147 (2015).
- ³⁵ T. Holstein, Ann. Phys. (N.Y.) **8**, 325 (1959); **8**, 343 (1959).
- ³⁶ R. T. Clay and R. P. Hardikar, Phys. Rev. Lett. **95**, 096401 (2005).
- ³⁷ R. P. Hardikar and R. T. Clay, Phys. Rev. B **75**, 245103 (2007).
- ³⁸ H. Fehske, G. Hager, and E. Jeckelmann, Europhys. Lett. **84**, 57001 (2008).
- ³⁹ H. Bakrim and C. Bourbonnais, Phys. Rev. B **91**, 085114 (2015).
- ⁴⁰ A. N. Rubtsov, V. V. Savkin, and A. I. Lichtenstein, Phys. Rev. B **72**, 035122 (2005).
- ⁴¹ R. P. Feynman, Phys. Rev. **97**, 660 (1955).
- ⁴² P. Werner and A. J. Millis, Phys. Rev. Lett. **99**, 146404 (2007).
- ⁴³ A. Schneider et al., Gnuplot-colorbrewer: ColorBrewer color schemes for gnuplot. Zenodo. 10.5281/zenodo.10282.
- ⁴⁴ A. C. Hewson and D. Meyer, J. Phys.: Condens. Matter **14**, 427 (2002).
- ⁴⁵ K. S. D. Beach, arXiv:0403055 (2004).
- ⁴⁶ S. Engelsberg and B. B. Varga, Phys. Rev. **136**, A1582 (1964).
- ⁴⁷ F. Michel and H. G. Evertz, arXiv:0705.0799.
- ⁴⁸ A. Migdal, J. Exp. Theor. Phys. **34**, 996 (1958).
- ⁴⁹ A. S. Alexandrov, V. V. Kabanov, and D. K. Ray, Phys. Rev. B **49**, 9915 (1994).
- ⁵⁰ Our field theory implies a continuum limit such that momentum conservation is exact. Hence the identification of $2k_F$ to $-2k_F$ for the half-filled band is not justified.
- ⁵¹ P. Lee, T. Rice, and P. Anderson, Solid State Commun.

14, 703 (1974).

⁵² B. Roy, V. Juričić, and I. F. Herbut, Phys. Rev. B **87**, 041401 (2013).

⁵³ T. C. Lang, Z. Y. Meng, A. Muramatsu, S. Wessel, and F. F. Assaad, Phys. Rev. Lett. **111**, 066401 (2013).

⁵⁴ We consider finite lattices with an arbitrary cutoff for the

phonons. The same results can be obtained by evaluating $\bar{B}(q, \omega) = \text{Im}[D(q, \omega + i\eta)]/\pi$ for the general case, where $D(q, z)$ has a branch cut on the real axis.

⁵⁵ In general, this need not be the case.

⁵⁶ However, the integrated weight $\int B(q, \omega)d\omega$ may be very different for $\omega < \omega_0$ and $\omega > \omega_0$.